Development of fibrillar texture during simultaneous biaxial drawing of ultra-high-molecular-weight polyethylene dried gels

Yoshihiro Sakai* and Keizo Miyasaka†
Department of Organic and Polymeric Materials, Tokyo Institute of Technology, Ookayama, Meguro-ku, Tokyo 152, Japan
(Received 9 December 1988; revised 1 February 1989; accepted 23 February 1989)

Simultaneous biaxial drawing of dried gel films of ultra-high-molecular-weight polyethylene (UHMW-PE) was followed by scanning electron microscopy (SEM) and other structural investigation techniques. The average width of fibrils estimated by SEM was an effective measure of the development of fibrillation. Regular microfibrillation almost finished at a draw ratio of (10 × 10) and further drawing seemed to be accomplished by slippage, entanglement and interception of microfibrils, breakage of some entangled microfibrils, as well as drawing of each fibril. These SEM observations correspond well to the changes in nitrogen gas permeability coefficient and in thermoluminescence glow with biaxial drawing. A field-emission SEM observation of the fracture face perpendicular to the film surface showed that thin layers less than 1 μm were formed during drawing, suggesting that biaxial extension was performed in each layer.

(Keywords: ultra-high-molecular-weight polyethylene; gel films; simultaneous biaxial drawing; thermoluminescence; gas permeability)

INTRODUCTION

High-modulus and high-strength fibre materials have been developed by high drawing of ultra-high-molecular-weight polyethylene (UHMW-PE). Gel spinning of material according to Smith and Lemstra[1–3] is considered as one of the best methods[4–9] of making high-performance materials, particularly from the productivity point of view. As a result, many studies have been made on the structure and properties of gel-drawn fibres, showing that they have a particular fine structure without any long spacing consisting of in-series crystalline and amorphous regions[10]. The fibre materials consist of microfibrils of several namometres in width which orient parallel to fibre axes, as revealed by scanning electron microscopy (SEM)[2,4,7,11–18] and transmission electron microscopy (TEM)[19,20]. The properties of these materials should depend on both intra- and interfibrillar structures. In our opinion, one of the most important reasons for the remarkable decrease in the modulus of highly drawn gel-spun UHMW-PE with increasing temperature[9,21] must be the deterioration of interfibrillar frictional property with heating. The particular structure without a long spacing makes it difficult to expect the modulus of fibrils to decrease as much as observed for the fibre. If the intrafibrillar structure is well described by an 'extended-chain' crystal mode[22–24], the temperature dependence of the modulus of fibrils must be negligible because the modulus of the crystal should be almost independent of temperature. Matsuo and Sawatari[25] expected a decrease in the modulus of the fibrils themselves, due to the decrease in crystallinity with heating.‡ They still recognized, however, that the decrease in the modulus of specimens is remarkable even after being compensated for the crystallinity.

Far fewer studies on biaxial drawing of UHMW-PE have been made than on uniaxial drawing. Minami and coworkers[26] attained a maximum draw ratio of (16 × 16) in their simultaneous biaxial drawing of UHMW-PE gel films. The maximally drawn film had a dynamic modulus of about 7 GPa at room temperature. In our previous paper[27], UHMW-PE films prepared by gelation according to Smith and Lemstra and by subsequent heat-compression at 150°C, which was higher than the melting point, were simultaneously biaxially drawn at 135°C to study the drawability of the film, and the structure and properties of drawn films, with the following results:

(1) The drawn film comprises microfibrils endlessly long and several tens of nanometres in width.

(2) They are not straight along their whole length and orient at random in the film plane.

(3) The fibrils form networks, referred to as 'fibrillar networks', whose junction points are made in two ways: 'ordinary junction points' at which two straight fibrils contact and cross each other, and 'fibrillar entanglements' formed by two deeply folded fibrils. If the latter type of fibrillar junction has once formed during drawing, the disentangling of fibrils must be difficult without breakage. Thus it may be said that this fibrillar entanglement is one of the most characteristic features of biaxial drawing of UHMW-PE gel films, and also one of the important reasons why it is difficult to get higher draw ratios than (16 × 16).

(4) As to the fine structure, the small-angle X-ray scattering (SAXS) peak due to the long spacing disappeared at a draw ratio about (10 × 10), suggesting a

* Research fellow from Kao Corporation
† To whom correspondence should be addressed

‡ The present authors do not always agree with their idea about the decrease in the modulus of fibres with heating: Is the crystalline and amorphous in-series structure valid in this gel-drawn UHMW-PE? Does the change in the (002) diffraction intensity with temperature reflect the change in the crystallinity?

0032-3861/90/010051-07$03.00

transformation of the crystalline–amorphous in-series structure into the structure with extended-chain crystals. These results showed the importance of the formation of fibrils (fibrillation) in simultaneous biaxial drawing of the material.

In this paper, simultaneous biaxial drawing of UHMW-PE films, prepared via gelation and heat-compression, is studied with particular interest in the origination and development of microfibrils, and in their related properties.

EXPERIMENTAL

Sample preparation

The sample material and preparation method were the same as in our previous paper[27]: UHMW-PE Hizex Million (Mitsui Petrochemical Co. Ltd) with $M_v = 4.5 \times 10^6$ was homogenized in a decahydronaphthalene solution containing 4 wt% polymer, using a separate flask at 160°C. Also 0.5 wt% (based on the polymer) of antioxidant, di-butyl-*p*-cresol, was added to the solution. The solution was cooled gradually to room temperature to make a gel. The gel was taken out of the flask and pressed between aluminium flat plates (coated with silver) under a pressure of 100 kg cm^{-2} at 150°C for 10 min, followed by quenching into water at 20°C. It should be pointed out that this sample preparation is different from that of the so-called dried gel films of Smith and Lemstra. In this case the film was formed by heat-compression of gel material instead of being formed as a gel sheet directly from the solution. Our method is not favourable because chain re-entanglement must occur more or less during heat-compression, resulting in less drawability. However, our method was better for making uniform sheets, which were absolutely necessary for biaxial drawing. It should be mentioned that 150°C was the best temperature for making sheets of uniform thickness. Thus prepared gel sheets were dried at room temperature, resulting in samples 0.11–0.13 mm thick. The structural aspects of the dried sheet were described in our previous paper. Samples of 10×10 cm^2 cut from the dried sheet were provided for simultaneous biaxial drawing performed at 135°C using an Iwamoto biaxial film stretcher.

Characterization methods

The SAXS intensity was measured using a scintillation counter with a pulse-height analyser and a vacuum camera with Ni-filtered Cu Kα radiation from a Rigaku Rota RU-200 working at 50 kV and 180 mA. Slit collimators 0.3–0.1 mm wide and 11 mm long were used in SAXS measurements.

The SEM observation was carried out for samples whose surfaces were coated with gold, using a Jeol JSM-350 SEM. In the measurements of the length of fibrils, SEM photographs were taken under a magnification of $\times 3500$, while higher magnifications were adopted in the measurements of fibril width. Samples fractured in liquid nitrogen were used for the field-emission scanning electron microscopy (FE-SEM) of their vertical face coated with platinum using a Hitachi S-800 FE-SEM. Nitrogen gas permeability of biaxially drawn UHMW-PE films was measured using an apparatus developed by Nakagawa[28]. Thermoluminescence (TL) measurements were carried out using the same apparatus and procedure as previously described[29]. A pile of drawn films whose thickness was about 8 μm was irradiated for 1 h at room temperature by the X-rays from the Cu target of a Riguka XG working at 35 kV and 20 mA, and then fixed to a copper sample-holder, which was set in a vacuum cryostat at a pressure of 10^{-3} torr. After free emission for 1 h at room temperature, the sample was heated at a rate of 6°C min^{-1}, during which the TL glow intensity was continuously measured.

RESULTS AND DISCUSSION

Figure 1 shows SAXS intensity curves, obtained by scanning in the plane defined by film thickness and the incident beam irradiated parallel to the film plane. The scattering intensities in *Figure 1* are normalized by the amount of films irradiated by X-rays. The curves in *Figure 1* correspond to the meridional scanning of the SAXS photographs in *Figure 5* in a previous paper[27]. Since fibrillar axes lie on the film plane while being oriented at random on the plane, the intensity curves in *Figure 1* give information about the width of fibrils.

As shown in *Figure 2*, the SAXS intensity curves obtained with the incident beam perpendicular to the film surface, which is naturally isotropic, showed the reverse tendency of change to those in *Figure 1*, i.e. the intensity curve tends to concentrate to the smaller

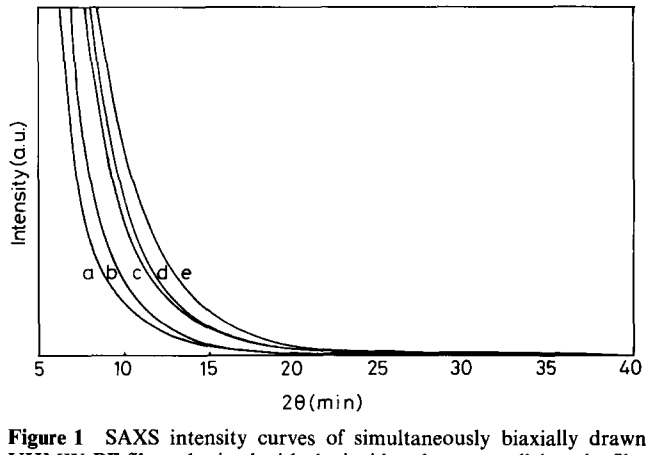

Figure 1 SAXS intensity curves of simultaneously biaxially drawn UHMW-PE films obtained with the incident beam parallel to the film plane, being scanned in the plane defined by the incident beam and the film thickness: (a) $\lambda = 4 \times 4$; (b) $\lambda = 6 \times 6$; (c) $\lambda = 10 \times 10$; (d) $\lambda = 12 \times 12$; (e) $\lambda = 16 \times 16$

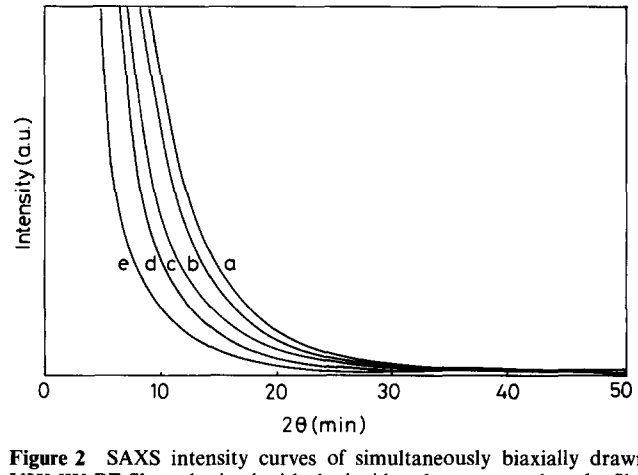

Figure 2 SAXS intensity curves of simultaneously biaxially drawn UHMW-PE films obtained with the incident beam normal to the film plane: (a) $\lambda = 4 \times 4$; (b) $\lambda = 6 \times 6$; (c) $\lambda = 10 \times 10$; (d) $\lambda = 12 \times 12$; (e) $\lambda = 16 \times 16$

scattering angle, which would suggest that the size of scattering bodies becomes larger with drawing. This peculiar change is supposedly due to the fact that void scattering prevails over fibrillar scattering. In any case, it is certain that the SAXS intensity curves obtained by the flat-on irradiation (through view) are difficult to use for estimation of the fibrillar width in this case.

The intensity curves of *Figure 1* tend to shift to wider scattering angle with increasing draw ratio, suggesting the thinning of fibrils. The fibril width was estimated using Hosemann's method[30] based on a Guinier relation given by:

$$I(s)=KNV^2\exp(-\langle R^2\rangle s^2) \quad (1)$$

with

$$s=(2\pi/\lambda)\sin(\chi/2)$$

where χ is the scattering angle, K is a constant depending on the measuring condition, N and V are the number and volume of scattering bodies, and $\langle R^2\rangle^{1/2}$ is the radius of gyration, which in this case corresponds to that measured in the cross section of a fibril. Thus the estimated radius of gyration $\langle R^2\rangle^{1/2}$ was reduced to the width of fibril W, using the following equation:

$$W=2(3\langle R^2\rangle)^{1/2} \quad (2)$$

This is valid for the case where X-ray irradiation is parallel to the thickness of a rectangular fibril with a width W, the same value of thickness W and infinite length. If a cylindrical fibril is assumed, the diameter of fibril D is related to $\langle R^2\rangle$ by:

$$D=2(2\langle R^2\rangle)^{1/2} \quad (3)$$

$\langle R^2\rangle$ is estimated from the slope of the ln $I(s)$ *versus* s^2 plot, while NV^2 is estimated from the intercept of the plot at $s=0$. Hosemann *et al.*[30] expanded the application of the equation to the case where fibrils with different $\langle R^2\rangle^{1/2}$ values coexist, and estimated the fibrillar width distribution in uniaxially drawn fibrous materials. *Table 1* shows fibril width thus estimated from the data in *Figure 1*, according to Hosemann's method.

Some additional explanation may be required with respect to *Table 1*. Hosemann's analysis of our data in *Figure 1* showed that fibrils were grouped into four species with widths indicated by *Table 1*. In *Table 1* the fourth group with the largest width becomes thinner with increasing biaxial draw ratio, while the widths of the other groups remain almost unchanged, i.e. group 3 at about 0.20 μm, group 2 at 0.10 μm and group 1 at 0.042 μm. Then it should be remarked that, although the representative values of width of these groups remain almost constant, the weight fraction of each group changes with drawing, as shown in *Figure 3*: the fraction of thinner group increases with draw ratio. It is interesting

Table 1 Fibril widths (μm) estimated from SAXS Guinier plot of simultaneously biaxially drawn UHMW-PE films

	Species			
Draw ratio	1	2	3	4
4 × 4	0.043	0.10	0.19	0.40
6 × 6	0.043	0.11	0.21	0.39
10 × 10	0.043	0.10	0.19	0.38
12 × 12	0.039	0.10	0.20	0.34
16 × 16	0.043	0.10	0.20	0.28

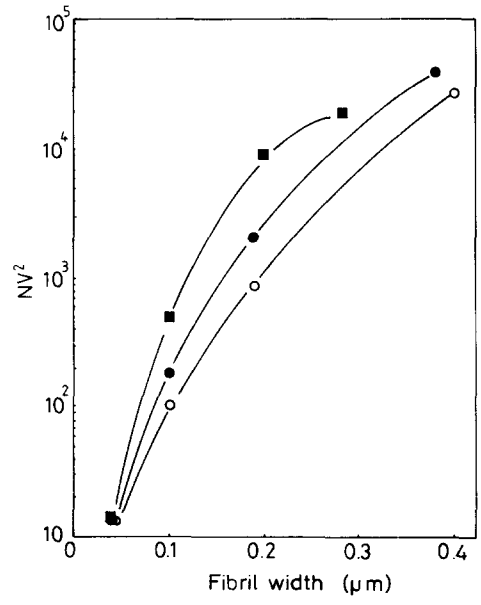

Figure 3 NV^2 in equation (1) vs. fibril width corresponding to *Table 1*: (○) $\lambda=4\times4$; (●) $\lambda=10\times10$; (■) $\lambda=16\times16$

to remind ourselves of the following facts: (1) the width estimated from SAXS corresponds to the width of fibril measured along the thickness of a drawn film, and (2) a very high degree of the crystal *a*-axis orientation parallel to the film thickness is caused in this drawn film, while the *c*-axis lies on the film plane[27]. These indicate that the width estimated here by SAXS corresponds to the width of fibril measured in the crystal *a*-axis direction. If the width had been able to be estimated reasonably from SAXS of the 'flat-on' irradiation (through view in *Figure 2*), the width should have corresponded to the width of fibril measured in the direction of the crystal *b* axis.

Next the width of fibrils was measured from SEM photographs taken for this purpose, such as shown in *Figure 4*. (It should be remarked that in a previous paper[27], the photographs in *Figures 9b* and *9c* should be interchanged.) According to *Figure 4*, the qualitative aspect of development of fibrils in this biaxial drawing was as follows. At a draw ratio of (4 × 4), fibrillar structure appears while the original particle structure still remains with a smaller size, having been consumed by the growth of fibrils. At a draw ratio of (10 × 10), the particle structure has completely transformed into a fibrillar one, with a small number of thick fibrils. At a draw ratio of (16 × 16), very thin fibrils seem to appear, and fibrillar networks develop. These observations are quantitatively evidenced by *Figure 5*, showing the fibrillar width evaluated from the SEM observation of surfaces of biaxially drawn films. It should be noted that the fibrillar width from SEM (*Figure 5*) corresponds to the width measured in the direction of the crystal *b* axis, according to the particular orientation modes of both crystals and fibrils as mentioned above. The weight distribution (given by the broken curve), which is shown in addition to the number distribution (full curve in *Figure 5*), was calculated under the assumption that fibrils have the same length and cylindrical shape whose diameter is given by the full curve of the number distribution. As expected from the modes of fibril and crystal orientation, fibrils must not be cylindrical, and,

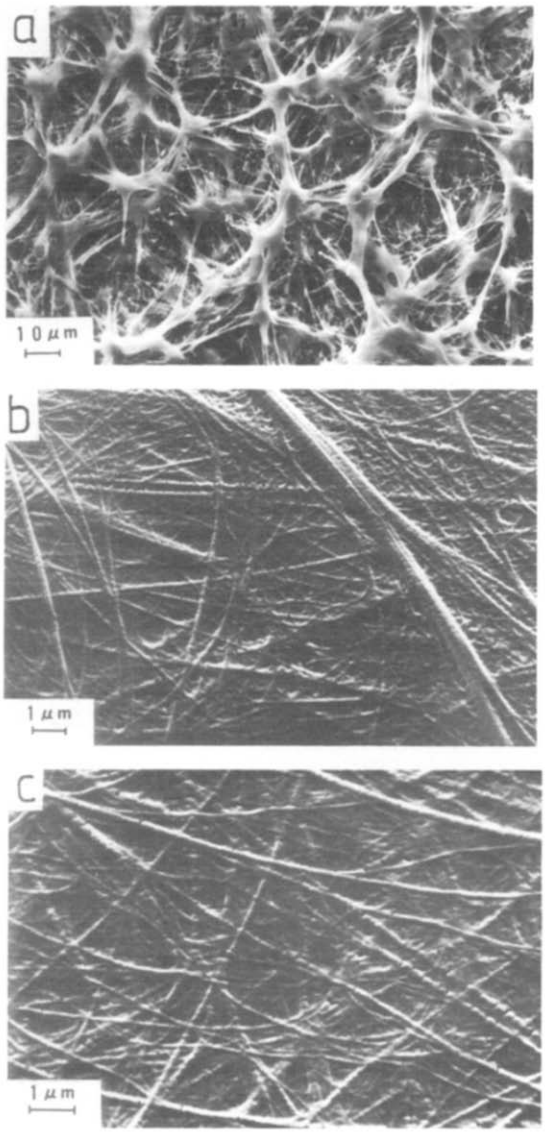

Figure 4 SEM photographs of simultaneously biaxially drawn UHMW-PE films: (a) $\lambda = 4 \times 4$; (b) $\lambda = 10 \times 10$; (c) $\lambda = 16 \times 16$

therefore, the validity of weight distribution must be much lower than that of number distribution.

At a draw ratio of (4×4), the number-average width is 0.29 μm, while the weight-average width is 0.69 μm. This big difference between the average width is attributed to the number distribution, which has a very long tail.*

At a draw ratio of (10×10), the number- and weight-average widths are 0.049 μm and 0.085 μm, respectively. This shows that such a great thinning as given by $(0.049/0.29) = 0.17$ is caused by drawing from (4×4) to (10×10). If each fibril is extended in an 'affine' mode, the ratio of width at (4×4) to that at (10×10) is approximately expected to be $(4/10)^{1/2} = 0.63$, which is much larger than the observed ratio 0.17. It is difficult to suppose that the draw ratio of each fibril is larger than that of the specimen. Splitting of each fibril effectively decreases the average width. It is, however, still difficult to explain this large discrepancy between 0.63 and 0.17, even if the possibility of splitting is taken into consideration. This implies that the value of average width at (4×4) must have been overestimated due to non-uniform fibrillation. At a draw ratio of (16×16), the number- and weight-average widths are 0.039 μm and 0.044 μm, and very thin fibrils about 0.02 μm in width newly appear, while thick fibrils larger than 0.2 μm almost disappear. The difference of number- and weight-average widths becomes very small, indicating an increased uniformity of fibril thickness between (10×10) and (16×16). The ratio of average width at (10×10) and (16×16), $(0.039/0.049) = 0.80$, is close to the ratio of $(10/16)^{1/2}$, suggesting that each fibril is extended in an 'affine' mode during drawing from (10×10) to (16×16). It should be remarked, however, that the structural change caused by drawing from (10×10) to (16×16) is not only thinning of each fibril but also the development of fibrillar networks. Slippage, splitting and entangling of fibrils are important at this high drawing, as well as thinning of each fibril by drawing. It should be noted that splitting of fibrils must be necessary for entangling of fibrils. Finally comparison of *Figure 5* with *Table 1* and *Figure 3* shows that the widths from SAXS are somewhat larger than those from SEM, although their orders of magnitude seem to coincide fairly well. This discrepancy between the widths estimated by different methods should be attributed only to the fact that SAXS followed less faithfully the change in the fibrillar width than SEM, but never to the dimensional anisotropy of cross section of each fibril which is expected from the

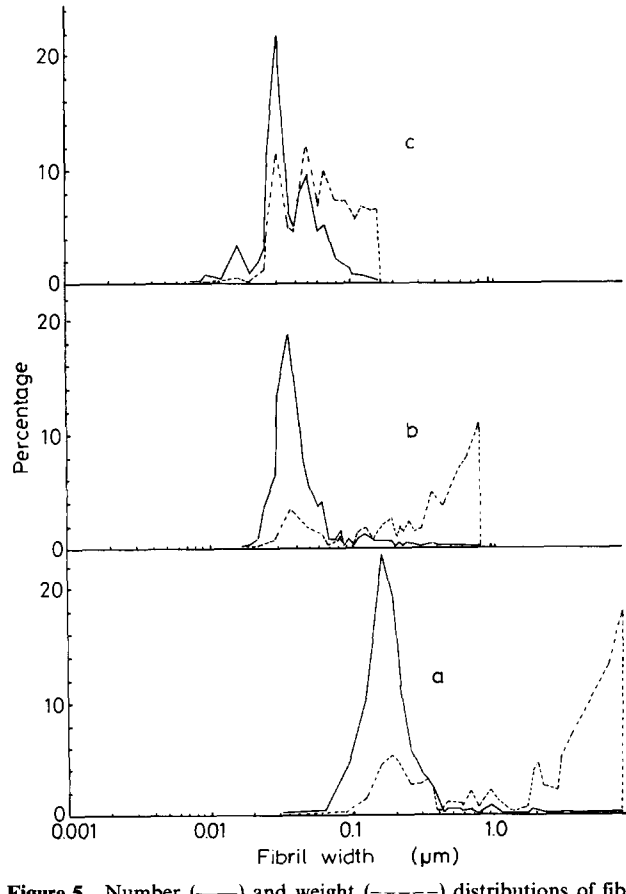

Figure 5 Number (——) and weight (– – – –) distributions of fibril width measured by SEM for simultaneously biaxially drawn UHMW-PE films: (a) $\lambda = 4 \times 4$; (b) $\lambda = 10 \times 10$; (c) $\lambda = 16 \times 16$

* According to Sakami *et al.*[12], the number- and weight-average width of fibrils measured by the same SEM method as ours were 0.12 μm and 0.26 μm, respectively, in a film prepared by (5×5) biaxial drawing in the molten state and subsequent cooling. Their values and the difference between them are smaller than ours for (4×4) drawing in this paper, which is due to the different mechanisms of fibril origination: crystallization in their case and cold drawing in our case.

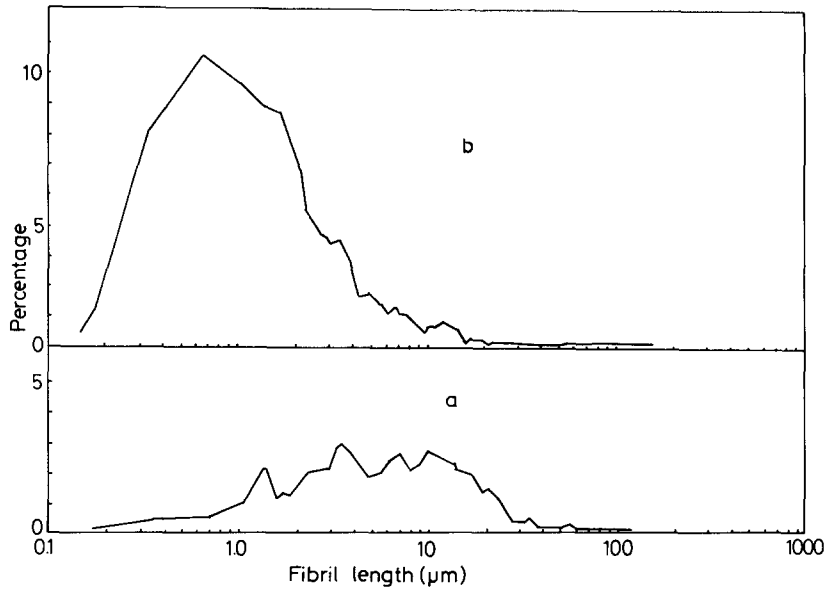

Figure 6 Fibril length measured by SEM for simultaneously biaxially drawn UHMW-PE films: (a) $\lambda = 10 \times 10$; (b) $\lambda = 16 \times 16$

particular modes of crystal and fibril orientation. *Figure 3* gives the fibril width measured in the direction of crystal *a* axis, while *Figure 5* gives the width measured in the direction of the *b* axis. It is reasonable to suppose that the width of fibril measured in the *b* axis direction is larger than that measured in the *a* axis direction, which is the reverse to what the comparison of *Figure 3* with *Figure 5* shows.

Figure 6 shows the fibril length at draw ratios of (10×10) and (16×16). The average length at (10×10) is 9.2 μm. The greatest length of fibril in this case may be equal to the product of the distance between centroids of the nearest particles about 10–15 μm in the original undrawn film, as shown in *Figure 9a* in a previous paper[27], and the draw ratio in one direction, i.e. 10 in the case of (10×10). Then the longest is about 150 μm at (10×10). It is interesting that the measured greatest length of fibril was 120 μm at (10×10), while the average value was 9.2 μm which was about one-tenth of the longest. The chain contour length corresponding to $M_w = 4.5 \times 10^6$ is about 40 μm, and therefore the average fibril length 9.2 μm is about one-quarter of the contour chain length. The fibril length at (16×16) further decreases to be smaller than one-tenth of that at (10×10). In the case of (16×16) the whole length of a fibril is very difficult to measure, because of the increased number of interception and entangling points of fibrils. Thus in this case the measured length of fibril does not correspond to the whole fibril length but to the length between two interceptions. The definition of fibril length is not the same between them. However, the difference of fibril length between (10×10) and (16×16) clearly shows how this drawing developed the fibril network texture, accompanying the increase in numbers of interception and entangling points.

Figure 7 shows the nitrogen gas permeability at room temperature as a function of biaxial draw ratio. The coefficient of the order of 10^{-11} before drawing increases to become of the order of 10^{-7} at a draw ratio of (4×4). This remarkable increase in the permeability corresponds well to the SEM observation, indicating the increase in porosity due to the irregular texture consisting

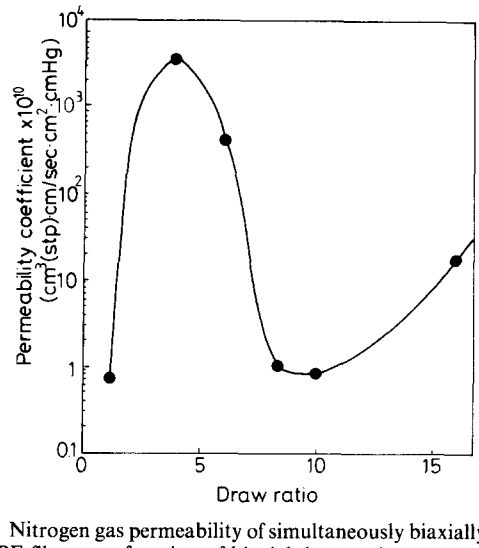

Figure 7 Nitrogen gas permeability of simultaneously biaxially drawn UHMW-PE films as a function of biaxial draw ratio

of fibrils and remaining particles. At a draw ratio of (10×10), the coefficient decreases to be restored to the 10^{-11} order of magnitude, corresponding to the increase in packing density of fibrils due to the increased structural regularity. According to SEM observation, films now comprise only fibrils which have become finer, and as a result the fibrillar texture is denser. It is interesting that the permeability coefficient again increases at draw ratios over (10×10). In a previous paper[27] we found not a small number of pairs of broken fibril ends which were supposed to be caused at entangling points. The small voids caused by the breakage of fibrils must be one of the reasons for the increased permeability. This indicates that high drawing necessarily accompanies the origination and development of voids.

It should be noted that in the drawing from (10×10) to (16×16) the modulus of the film increases montonically with increasing draw ratio[27], whereas the increase in porosity is suggested by the increase in permeability. This means that the hardening and straightening of fibrils themselves overcome the softening as suggested by the re-increased permeability.

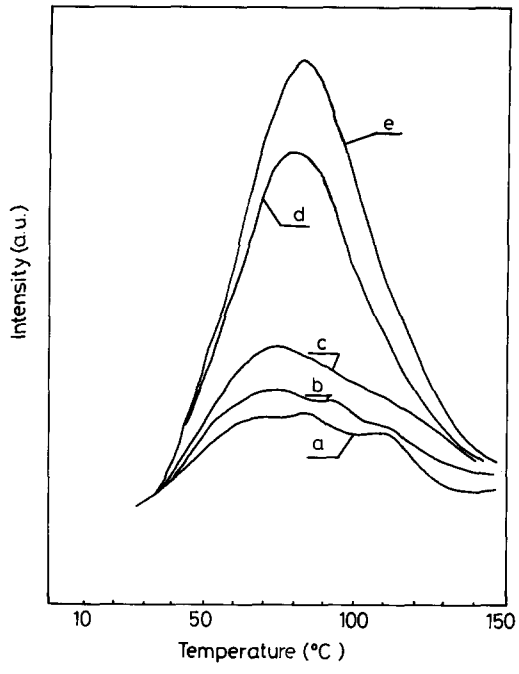

Figure 8 TL glow curves of simultaneously biaxially drawn UHMW-PE films as a function of biaxial draw ratio: (a) $\lambda = 1 \times 1$; (b) $\lambda = 4 \times 4$; (c) $\lambda = 6 \times 6$; (d) $\lambda = 10 \times 10$; (e) $\lambda = 16 \times 16$

Figure 8 shows the change of TL glow curves with biaxial drawing of UHMW-PE films. The peaks with their maxima at about 70–80°C correspond to the so-called α_c mechanical dispersion related to the crystalline region, i.e. frictional properties within a crystal[31] and at the boundary of crystals[32]. The TL glow of UHMW-PE gel films was first studied by our group[33,34] to show that the TL glow relating to the α_c mechanical dispersion increases its intensity remarkably with increasing draw ratio. The enhancement of TL glow showed that a great number of defects as the trap sites for electrons are introduced during high drawing. The extraordinarily strong TL intensity is considered to be one of the important structural characteristics of the ultra-highly drawn UHMW-PE. The enhanced TL glow is seen also in this case of biaxial drawing, as is shown in *Figures 8* and *9* where the integrated intensity is shown as a function of draw ratio. It is interesting in *Figure 9* that the TL intensity increases remarkably between (6×6) and (10×10), and the enhancement seems to become milder at draw ratios over (10×10). Since the increase in the TL glow is supposedly mainly due to the origination of defects within a fibril, the enhancement becomes remarkable when fibrils themselves are drawn, changing their fine structure. Experimental results on changes of SAXS[27] and width of fibrils suggested that further drawing over (10×10) is accomplished not only by drawing of the fibrils themselves but by additional changes in the fibrillar network texture which are related to their slippage, entanglement and interception. The TL glow in *Figure 9* supports these suggested mechanisms of biaxial drawing of UHMW-PE gel films.

FE-SEM photographs of the vertically fractured face on which the thickness of biaxially drawn film lies are shown in *Figure 10*. *Figure 10a* for (4×4) specimen shows that thin layers less than 1 μm in thickness are formed, being stacked. This is important because it shows that biaxial drawing proceeds in each thin layer. The (16×16) photograph (*Figure 10b*) does not show any real structure in the vertical cross section of the highly drawn film. We attempted to get a better fracturing of (16×16) sample for SEM observation using various methods, but failed. The faces shown in *Figure 10* were prepared by fracturing films in liquid nitrogen. It is interesting that in *Figure 10b* the fractured face consists of a ball-like structure, which makes us suppose that each fibril melted at breakage of films in liquid nitrogen.

SUMMARY

Simultaneous biaxial drawing of dried gel films of UHMW-PE was studied, with the following results.

(1) In this case, the estimation of fibril width by SAXS by flat-on irradiation (through view) was impossible mainly because of the large effect of void scattering, while possible by parallel irradiation SAXS (edge view).

(2) The estimation of fibril width by SEM was effectively made, although it was difficult to get a correct value because of the irregularity of fibrillation at low draw ratios.

(3) The fibrillar texture was accomplished at a draw

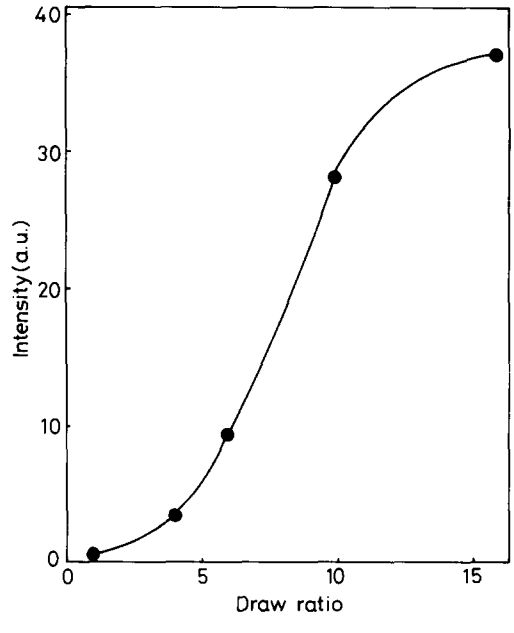

Figure 9 Integrated TL intensity of simultaneously biaxially drawn UHMW-PE films as a function of biaxial draw ratio

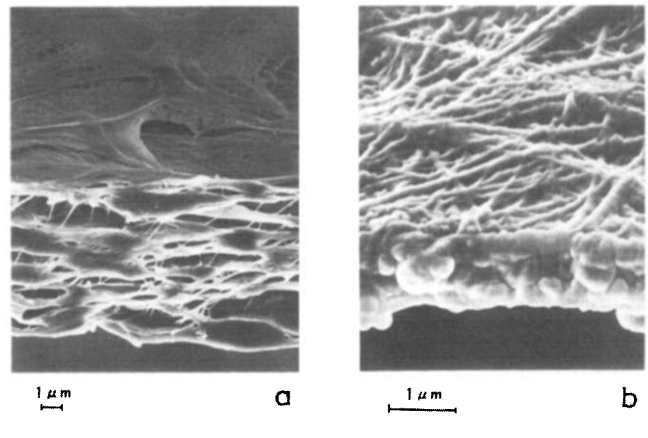

Figure 10 FE-SEM photographs of the fracture face, on which the film thickness lies, of simultaneously biaxially drawn UHMW-PE films: (a) $\lambda = 4 \times 4$; (b) $\lambda = 16 \times 16$. Sample films were fractured in liquid nitrogen

ratio of about (10×10) and further drawing seems to accompany slippage, entanglement, interception and breakage of fibrils, as well as thinning of each fibril.

(4) The changes in the permeability coefficient of nitrogen gas and in TL glow intensity were effective to follow the structural change caused by biaxial drawing.

(5) An FE-SEM observation showed that thin layers less than 1 μm in thickness and parallel to the film surface were formed during biaxial drawing.

REFERENCES

1 Smith, P. and Lemstra, P. J. *Makromol. Chem.* 1979, **180**, 2983
2 Smith, P. and Lemstra, P. J. *J. Mater. Sci.* 1980, **15**, 505
3 Smith, P. and Lemstra, P. J. *Polymer* 1980, **21**, 1341
4 Zwijnenburg, A. and Pennings, A. J. *Colloid Polym. Sci.* 1976, **254**, 868
5 Pennings, A. J. and Torfs, J. *Colloid Polym. Sci.* 1979, **257**, 547
6 Barham, P. J. and Keller, A. *J. Mater. Sci.* 1980, **15**, 2229
7 Smook, J., Torfs, J. C., Hutten, P. F. and Pennings, A. J. *Polym. Bull.* 1980, **2**, 293
8 Smith, P. and Lemstra, P. J. *Colloid Polym. Sci.* 1980, **258**, 891
9 Furuhata, K., Yokokawa, T. and Miyasaka, K. *J. Polym. Sci., Polym. Phys. Edn.* 1984, **22**, 133
10 Pennings, A. J., Smook, J., Boer, J., Gogolewski, S. and Hutten, P. F. *Pure Appl. Chem.* 1983, **55**, 777
11 Zwijnenburg, A. and Pennings, A. J. *Polym. Lett.* 1976, **14**, 339
12 Sakami, H., Iida, S. and Sasaki, K. *Kobunshi Ronbunshu* 1977, **34**, 653
13 Smook, J., Flinterman, M. and Pennings, A. J. *Polym. Bull.* 1980, **2**, 775
14 Kalb, B. and Pennings, A. J. *Polym. Commun.* 1980, **21**, 3
15 Pennings, A. J. and Zwijnenburg, A. *J. Polym. Sci., Polym. Phys. Edn.* 1979, **17**, 1011
16 Smith, P., Lemstra, P. J., Pijpers, J. P. L. and Kiel, A. M. *Colloid Polym. Sci.* 1981, **259**, 1070
17 Smith, P., Chanzy, H. D. and Rotzinger, B. P. *Polym. Commun.* 1985, **26**, 258
18 Zachariades, A. E. and Kanamoto, T. *J. Appl. Polym. Sci.* 1988, **35**, 1265
19 Hutten, P. F., Koning, C. E., Smook, J. and Pennings, A. J. *Polym. Commun.* 1983, **24**, 237
20 Sakami, H. *Kobunshi Ronbunshu* 1987, **44**, 477
21 Matsuo, M. and Sawatari, C. *Macromolecules* 1987, **20**, 1745
22 Wunderlich, B., Comier, C. M., Keller, A. and Machin, M. J. *J. Macromol. Sci.–Phys. (B)* 1967, **1**, 93
23 Pennings, A. J., Mark, J. M. A. A. and Keil, A. M. *Kolloid Z. Z. Polym.* 1970, **237**, 336
24 Sakami, H. and Ideisi, T. *Kobunshi Ronbunshu* 1979, **36**, 575
25 Matsuo, M. and Sawatari, C. *Macromolecules* 1988, **21**, 1653
26 Minami, S. and Itoyama, K. *Polym. Prepr.* 1985, **26**(2), 245
27 Sakai, Y. and Miyasaka, K. *Polymer* 1988, **29**, 1608
28 Nakagawa, T. *Kogyogijutsu* 1965, **6**(2), 20
29 Liu, L. B., Hiyama, K. and Miyasaka, K. *Polymer* 1988, **29**, 286
30 Bonart, R. and Hosemann, R. *Kolloid Z. Z. Polym.* 1962, **186**, 16
31 Takayanagi, M., Aramaki, T., Yoshino, M. and Hoashi, K. *J. Polym. Sci.* 1960, **46**, 531
32 Tanaka, A., Chang, E. P., Delf, B., Kimura, I. and Stein, R. S. *J. Polym. Sci., Polym. Phys. Edn.* 1973, **11**, 1891
33 Zhang, F. S., Murakami, N., Yokokawa, T. and Miyasaka, K. *Polym. Prepr. Japan* 1986, **35**(10), 3584
34 Liu, L. B., Murakami, N., Sumita, M. and Miyasaka, K. *Polym. Prepr. Japan* 1988, **37**(8), 2375